Energy Storage Materials 30 (2020) 329–336

Contents lists available at ScienceDirect

Energy Storage Materials

journal homepage: www.elsevier.com/locate/ensm

In-situ fabrication of carbon-metal fabrics as freestanding electrodes for high-performance flexible energy storage devices

Xinhua Liu [a], Mengzheng Ouyang [a], Marcin W. Orzech [c], Yubiao Niu [c], Weiqiang Tang [a,d], Jingyi Chen [a], Max Naylor Marlow [a], Debashis Puhan [a], Yan Zhao [b], Rui Tan [a], Brankin Colin [a,e], Nicholas Haworth [a], Shuangliang Zhao [d], Huizhi Wang [a], Peter Childs [a], Serena Margadonna [c], Marnix Wagemaker [f], Feng Pan [b,*], Nigel Brandon [a], Chandramohan George [a,**], Billy Wu [a,***]

[a] Imperial College London, SW7 2AZ, London, UK
[b] Peking University Shenzhen Graduate School, 518055, Shenzhen, China
[c] Swansea University, Swansea, SA1 8PP, UK
[d] State Key Laboratory of Chemical Engineering and School of Chemical Engineering, East China University of Science and Technology, Shanghai, 200237, China
[e] Department of Chemical and Biomolecular Engineering, University of Notre Dame, 46556, Indiana, USA
[f] Department of Radiation Science and Technology, Delft University of Technology, Delft, Netherlands

A R T I C L E I N F O

Keywords:
Carbon-metal fabrics
Non-woven
Electrospinning
Nanofibers
Carbon
Metal-air batteries
Flexible batteries

A B S T R A C T

Hierarchical 1D carbon structures are attractive due to their mechanical, chemical and electrochemical properties however the synthesis of these materials can be costly and complicated. Here, through the combination of inexpensive acetylacetonate salts of Ni, Co and Fe with a solution of polyacrylonitrile (PAN), self-assembling carbon-metal fabrics (CMFs) containing unique 1D hierarchical structures can be created via easy and low-cost heat treatment without the need for costly catalyst deposition nor a dangerous hydrocarbon atmosphere. Microscopic and spectroscopic measurements show that the CMFs form through the decomposition and exsolution of metal nanoparticle domains which then catalyze the formation of carbon nanotubes through the decomposition by-products of the PAN. These weakly bound nanoparticles form structures similar to trichomes found in plants, with a combination of base-growth, tip-growth and peapod-like structures, where the metal domain exhibits a core(graphitic)-shell(disorder) carbon coating where the thickness is in-line with the metal-carbon binding energy. These CMFs were used as a cathode in a flexible zinc-air battery which exhibited superior performance to pure electrospun carbon fibers, with their metallic nanoparticle domains acting as bifunctional catalysts. This work therefore unlocks a potentially new category of composite metal-carbon fiber based structures for energy storage applications and beyond.

1D carbon based structures such as carbon nanotubes (CNT) and carbon nanofibers (CNF) are attractive due to their continuous nature, chemical stability and the ability to be functionalised which are advantageous in a range of applications [1,2]. However, despite their promise, they suffer from manufacturing issues due to their desired structures requiring many fabrication steps, such as functionalisation, surface conditioning and coating. Since the discovery of CNTs [3], many types of carbon structures, composites and hybrids have been developed and exploited in applications including lithium-ion (Li-ion) batteries [4,5], energy conversion and catalysis [6,7]. In particular, 1D carbon based structures [8] across different length scales built into 3D scaffolds have shown attractive performance, for example, carbon papers for proton exchange membrane fuel cells [9], CNFs for supercapacitors [10], lithium-sulphur batteries [11] and metal-air batteries [12]. Each length scale of interest offers certain advantages. Macro-scale fibers offer ease of fabrication and good electronic conductivity, submicron scale features exhibit good electrochemical performance, and nano-scale tubes provide enhanced mechanical properties. Thus, the potential of synthesising hierarchical carbon based structures that integrate the above multi-length scale characteristics into a single material is extremely attractive.

* Corresponding author.
** Corresponding author.
*** Corresponding author.
E-mail addresses: panfeng@pkusz.edu.cn (F. Pan), chandramohan.george@imperial.ac.uk (C. George), billy.wu@imperial.ac.uk (B. Wu).

https://doi.org/10.1016/j.ensm.2020.04.001
Received 4 November 2019; Received in revised form 29 February 2020; Accepted 1 April 2020
Available online 25 April 2020

Various methods exist to synthesize these structures which includes the deposition of nano-scale catalyst particles onto substrates and subsequent growth of CNTs via processes such as chemical vapour deposition (CVD) which, whilst effective, are expensive and time consuming. On the other hand, electrospinning is a well-developed and industrially adopted process for manufacturing carbon fibers [13–15]. In this process a polymer and solvent, such as polyacrylonitrile (PAN) in N, N-dimethylformamide (DMF), is extruded through a nozzle and spun into micron to nano sized fibers via the application of a high voltage electric field. The subsequent fibers are then pyrolysed at high temperatures to produce carbon structures. Based on this technique, carbon mats, felt and fabrics with non-woven fibers have been produced and exploited as separators and electrodes in Li-ion batteries [16,17], binderless anodes with MoS_2 for sodium ion batteries [18], cathodes for zinc-air batteries [19,20] and as supercapacitor electrodes when combined with metal-oxides [21]. Although electrospinning is capable of producing free-standing structures, most of them do not span multiple length scales and thus do not exploit the potential material properties. For example, electrospun fabrics tend to be fragile and mechanically weak and with a small surface area compared to other forms of carbon. To mitigate this, approaches such as incorporating nanoparticles to improve surface area [22,23], electro-netting with a polymer, carbon, titanium oxide [24] to improve electronic conductivity and deposition of palladium nanoparticles and consequent CNT growth to make secondary fibers [25] with catalytic functions have been developed.

Recently, Yao et al. have reported an important breakthrough by exploiting a carbothermal shock synthesis route which enabled the production of multicomponent nanoparticles (high entropy alloys) on carbon nanofibers, exhibiting remarkable catalytic properties which highlighted the potential of functionalising CNFs [26]. Although some progress has been made in preparing hierarchical nanocomposites and in understanding the associated CNT and CNF growth mechanisms, current manufacturing routes are still expensive and complex. For example, Fe3C@NCNTs-NCNFs were prepared in the presence of melamine as carbon source with costly Ar flow [27]; CNT−CNF–Ni hybrid materials were pyrolysed in H_2/N_2 (5%/95%) and then heated in vacuum to grow CNTs by introducing Poly(methyl methacrylate) as a carbon source [28, 29].

Thus, motivated by this, we present a scalable synthesis route for hierarchical CNFs with catalytically active metal nanoparticle domains through the modification of existing industrial techniques. The applicability of this material is demonstrated as a bifunctional cathode for a zinc-air battery which exhibits mechanical robustness, flexibility and stable performance with the potential to be transferred into other applications.

Drawing inspiration from trichomes, the fine bristle like micro-nano structures found in certain plants and insects, we present an architectural material that can integrate material functionalities at different length scales (nano-micro-macro), which we term carbon metal fabrics (CMFs). By combining electrospinning and a floating catalyst pyrolysis synthesis route, we demonstrate a scalable and tractable production method for CMFs that produces hierarchical morphologies ideal for energy storage applications. These CMFs consist of micron-sized electrospun non-woven carbon fibers covered in bristles of carbon nanotubes that encase catalytically active metal nanoparticles (Fe, Ni and Co). Our structural, spectroscopic and microscopic analysis of these CMFs present new insights into the microstructural features of these carbon-metal composites, highlighting unique features conducive to development of high performance energy-storage devices as well as understanding their synthesis mechanisms. As a proof of concept, we designed and fabricated a series of flexible Zn-air batteries using these CMFs. The battery performance in terms of current density, capacity and capability further underpins the benefits of these hierarchical composite nanocarbon, metal nanoparticles and carbon fiber materials as battery electrodes.

A tractable manufacturing route for non-woven CMFs has been developed by combining electrospinning and pyrolysis. The non-woven electrospun fibers, which serve as the skeleton for the CMFs, are approximately 600 nm in diameter and have lengths in the centimetre length scale. Detailed fabrication methods and procedures are provided in the supporting information. In brief, organometallic salts (acetylacetonate forms of Fe, Co or Ni) were mixed with a polymer solution of PAN in DMF. Electrodes with thicknesses of up to 500 μm were fabricated by controlling the electrospinning time. These electrospun fibers were then subjected to a stabilisation process at 290 °C in air for 2 h and a pyrolysis step at 850 °C in nitrogen (N_2), where the organometallic salts (Fe, Ni or Co) decompose at temperatures of approximately 170 °C. This gives rise to the formation of well-faceted metal nanoparticles through an exsolution mechanism, which are randomly distributed on the surface of the electrospun fibers (Fig. 1). Control experiments during heat treatment show the gradual emergence of Fe, Co and Ni nanoparticles during stabilisation and carbonisation across the fibers (Figs. S1–S3). This carbonisation method where the catalyst precursors are introduced in the initial electrospinning solution is known as floating catalysis, meaning that catalyst particles are self-assembled *in situ* during the heat treatment process, as opposed to other methods where catalysts are applied directly as nanoparticles at the start of the reaction or after CNF synthesis (Table S1). As a result, the newly formed catalyst particles tend to freely diffuse and migrate to the surface of the CNF to minimise their free energy leading to the growth of secondary CNTs. Evidently, the appearance of carbon nanotubes like bristle or hairs on the primary electrospun fibers at temperatures above 600 °C is caused by the presence of catalyst particles which exhibit a combination of base growth, tip growth and peapod like CNT structures as shown in Fig. 1 and the supporting information. Most of the carbonised electrospun fibers run parallel whilst some crisscross, serving as primary scaffoldings for the CMFs, which can then be reinforced by the presence of bristle like growth of carbon nanotubes capable of interlocking the fibers when in contact (similar to Velcro). Such an arrangement further imparts the fabrics with robustness and mechanical pliability, whilst the infiltration of metal either as elongated nanoparticles or rods into the bristle like CNTs provide additional structural support. The resulting structure is a free standing CMF with mechanical flexibility, capable of being rolled and even twisted (see later).

Fig. 2 shows the high-angle annular dark-field- scanning transmission electron microscope (HAADF-STEM) images of all the three CMFs (Fe, Co, and Ni). In many nanotubes, metal in the form of nanorods infiltrates the CNTs, which may be the reason for the growth of peapod like structures (Fig. S4) depending on the local kinetics and strain. For most of the Ni and Co based nanotubes, the metal nanoparticles exhibited "peapod" type structures (Figs. S4–S5), with multiple graphitic layers, which are an intermediate growth mechanism between the typical tip and base growth modes. In most of the cases, the metal nanoparticle domains found at the tip of the tubes are covered by either thick (15 nm) or thin (3 nm) carbon shells. These regions consist of well-crystallised metal particles (~40–60 nm) which are encapsulated in graphitic/ disordered carbon layers, as shown by high resolution transmission electron microscopy (HRTEM) (Fig. 2). Interestingly, the Fe-based fabrics generally have thinner carbon coatings, with these being mostly graphitic.

To gain insights into the chemical composition of these fabrics, Energy-dispersive X-ray spectroscopy (EDS) analysis was performed. The TEM images in Fig. 3 show a homogenous distribution of carbon in the electrospun fibers (Fig. 3a, c, 3e) and the presence of metals (Fe, Co or Ni) as nanoparticles from which bristle like carbon nanotube had grown. A focused-ion beam scanning electron microscope (FIBSEM) reconstruction movie is presented in the supporting information and shows the presence of metal particles both on the surface and bulk of electrospun fibers. The presence of the carbon shell around the Co and Ni domains and thin shells around the Fe nanoparticles can be distinguished from this mapping (Fig. 3b, d, 3e). When measuring the intensity of the carbon signals in the nanoparticle region, the intensity for the Fe based fabrics is lower than that of the Co and Ni, further confirming the thinner carbon coating.

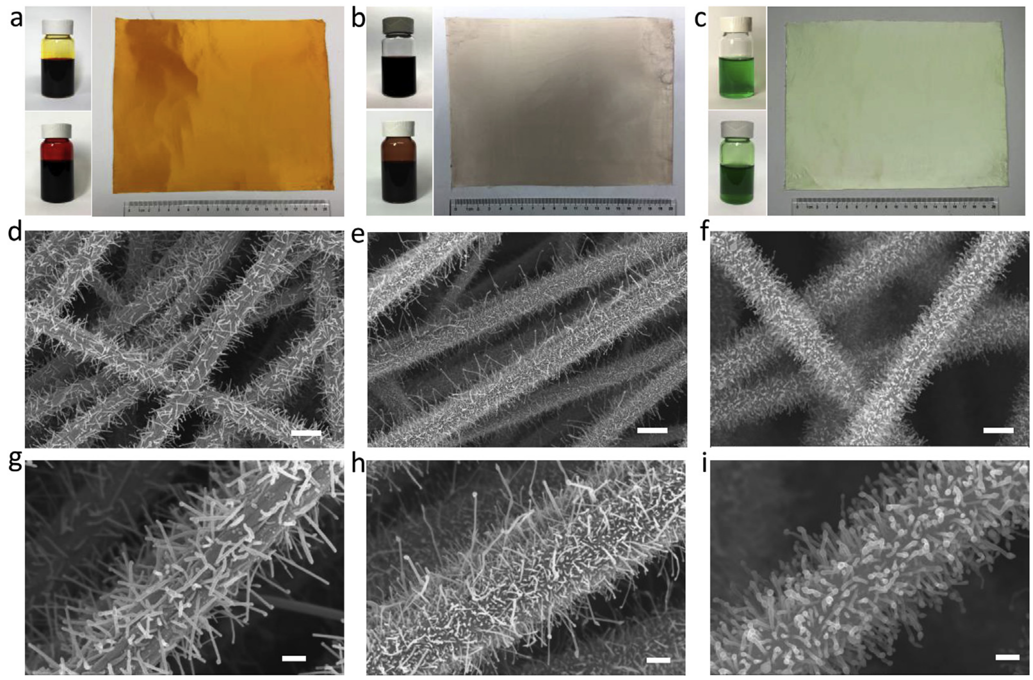

Fig. 1. SEM images of hairy fibers. Mixed solutions in bottles: $M(acac)_X$ + DMF (upper), $M(acac)_X$ + DMF + PAN (lower), and their electrospun nanofiber films. a, M = Fe, x = 3, $Fe(acac)_3$, b, M = Co, x = 2, $Co(acac)_2$, c, M = Ni, x = 2, $Ni(acac)_2$. d, g, SEM images of Fe based hairy carbon nanofiber. e, h, SEM images of Co based hairy carbon nanofiber. f, i, SEM images of Fe based hairy carbon nanofiber. (The scale bar in 1 μm for d, e, f and 200 nm for g, h, I).

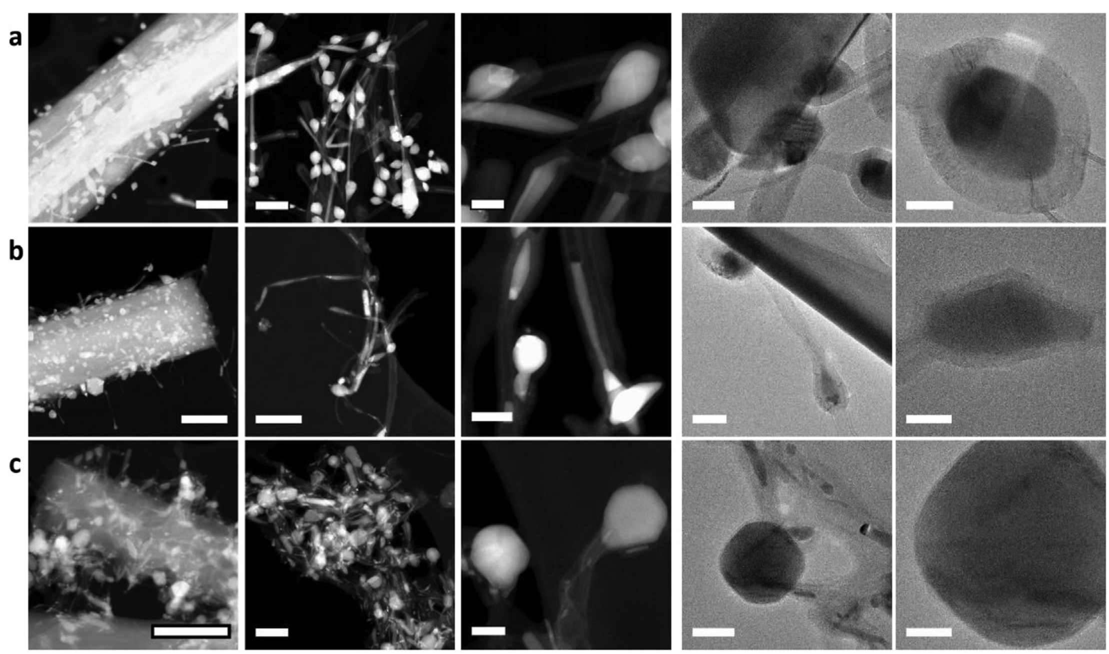

Fig. 2. High-angle annular dark-field (HAADF-STEM) and high resolution TEM images of carbon metal fabrics (CMFs). a, Ni based CMFs. b, Co based hairy carbon nanofiber. c, Fe based CMFs. The first image in each row shows larger carbon nanofiber, while the following zoom in on the "bristles" and encapsulated metal nanoparticles. The scale bars in each column starting from left are 400 nm, 200 nm, 50 nm, 50 nm and 20 nm respectively.

Supplementary video related to this article can be found at https://doi.org/10.1016/j.ensm.2020.04.001.

The X-ray diffraction (XRD) patterns obtained on these fabrics are presented in Fig. S6 which further confirms the presence of carbon and the metallic phase in the CMFs across the varied mass ratios of precursors from 30% wt to 50 wt%. The (0 0 2) Bragg's peak for carbon indicates the presence of both graphite and amorphous carbon in all fibers which is line with the TEM measurements in Figs. 2 and 3. In both Figs. S6a and S6b, the pure metallic phase of Ni and Co can be identified. In Fig. S6c, the Bragg's peaks in the Fe fibers indicates the presence of phases other than pure Fe and C. On the Fe40 pattern (Fe40, post carbonised from electrospun nanofiber with 40 wt% $Fe(acac)_3$), Le Bail refinement was carried out using the P n m a(63) space group for Fe_3C cementite having an orthorhombic structure (Fig. S6d). The Chi [30] for the Le Bail refinement was found to be 1.15 which suggests that the Fe and C have reacted to form cementite during the heat treatment. From the XRD patterns, the crystallite

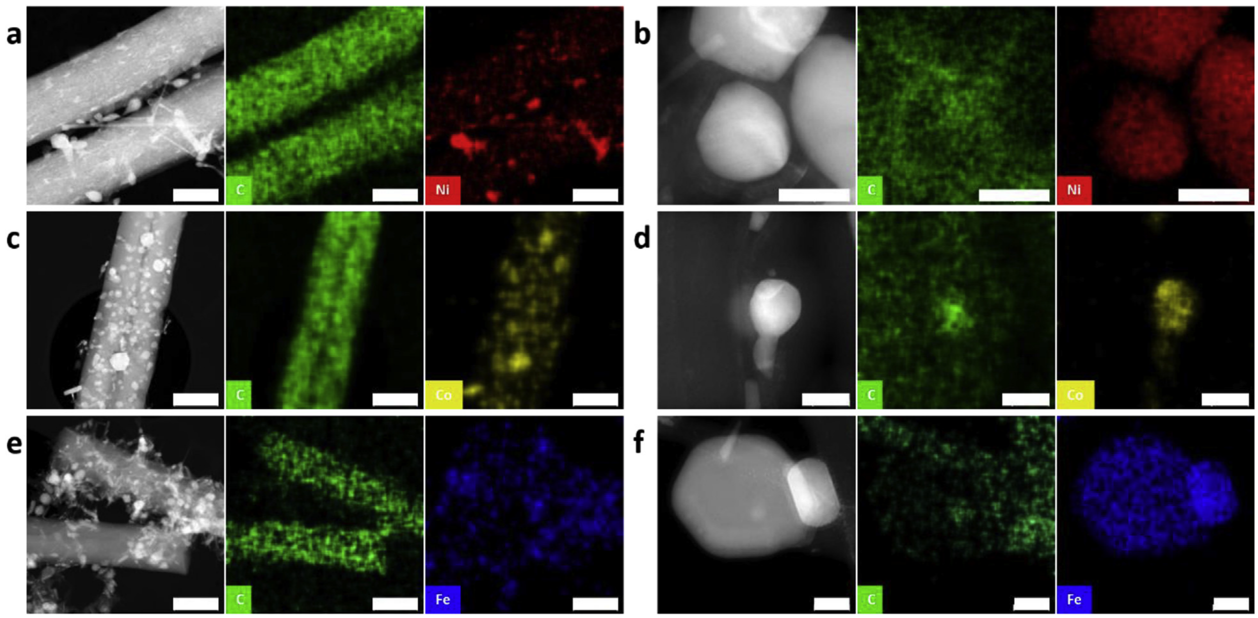

Fig. 3. Elemental composition of the hairy fibers. a-f, STEM images for elemental mapping by energy-dispersive spectroscopy of Ni (a–b), Co (c–d) and Fe (e–f) based hairy carbon nanofibers. a,c,e, Lower magnification of larger carbon nanofiber covered with "hairs". b,d,f, Magnified Ni, Co and Fe nanoparticles enclosed in nanotubes. (The scale bar is 400 nm and 40 nm in a,c,e and b,d,f, respectively.)

sizes for the metallic phases were found to be approximately 20 nm, which is in line with TEM measurements. The calculations based on the C (0 0 2) peak position for the Co and Ni fibers show the highest degree of graphitisation, whilst this could not be accurately calculated for the Fe fibers due to overlapping of the Fe_3C peaks and C (0 0 2) in the XRD patterns. In both the Ni and Co fibers, the samples with 40% metal loading showed the highest degree of graphitisation (Table S2). A detailed XPS analysis performed on these samples confirms the metallic nature of the nanoparticles and graphitic carbon with pyridine Nitrogen (Fig. S7).

Growth Mechanism of the CMFs. In the pre-carbonisation process, metal oxide nanoparticles are formed in the nanofibers from the metal salt additives, which are then reduced to form metal domains upon further heat treatment. These nanoparticles diffuse to the surface of the CNFs through an exsolution mechanism resulting in a nanoparticle decorated CNF. Given that the subsequent carbonisation was carried out under a N_2 atmosphere with no additional carbon source present, it is proposed that the feedstock for growth of the CNT "bristles" were the by-products of the thermal decomposition of PAN, which includes carbon species such as CH_4 and CO [31]. These gases are decomposed *in-situ* leading to the deposition of carbon at the nanoparticle surface, leading to the formation and growth of the CNT "bristles". Fig. 4 shows the proposed route for the growth of carbon nanotubes on electrospun fibers

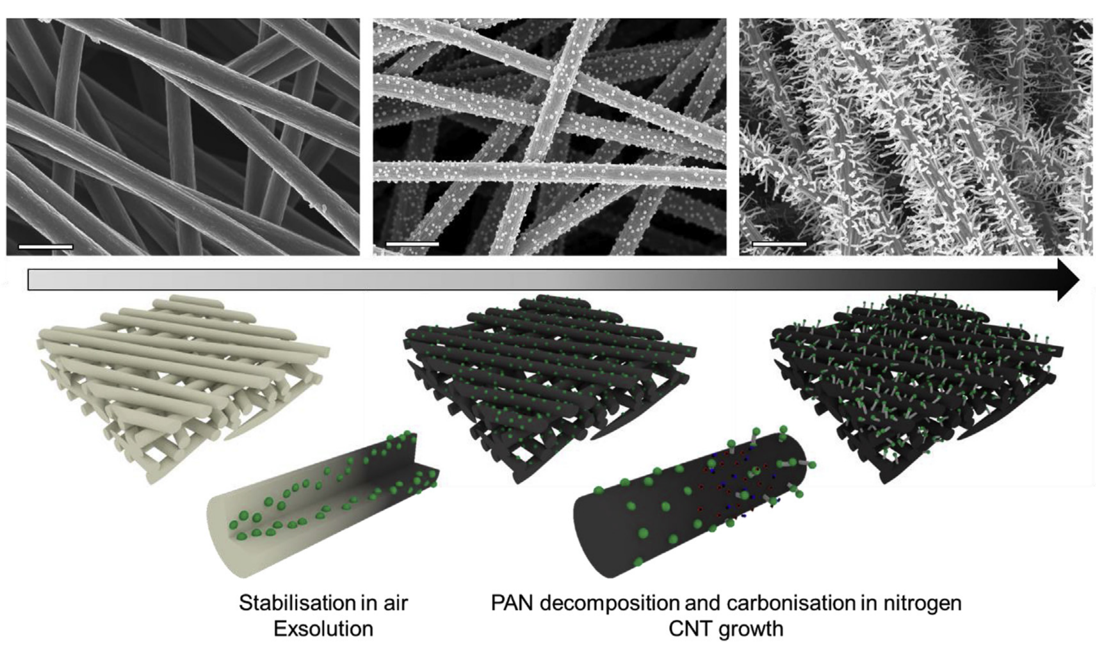

Fig. 4. SEM and diagrammatic representation images of the various stages of synthesis for the CMFs. Light fibers represent uncarbonised PAN, green particles are catalyst particles and dark fibers are stabilised and carbonised fibers. Scale bar = 2 μm. (For interpretation of the references to colour in this figure legend, the reader is referred to the Web version of this article.)

leading to CMFs, which is in line with control experiments performed at lower temperatures.

For example, the SEM images of the surface morphology of the Fe based electrospun nanofibers with different heat treatment stages are shown in Fig. S1. Compared to electrospun fibers before carbonisation, small nanoparticles are formed after pre-carbonisation, where these small nanoparticles tend to form larger nanoparticles at higher temperatures of 550 °C, with the "bristle" found with further heat treatment to 850 °C. The same trends can also be found in Co and Ni based carbon nanofibers (Figs. S2 and S3). As evidenced in the TGA results (Fig. S8), the slight mass decrease of the metal salt precursors at temperatures below 200 °C was due to the loss of absorbed free water and bound water. The thermal decomposition after 200 °C was rapid, resulting in a dark precipitate. According to the literature [32], nanoscale Fe, Co and Ni oxides (Fe_3O_4, CoO and NiO) can be obtained. Therefore, nano-dimensional metal oxides can be obtained by the decomposition of their metal salt precursors during the stabilisation of the electrospun nanofibers. This reaction is terminated after 400 °C, but a pre-carbonisation temperature of 290 °C was selected for the consideration of good stabilisation of the PAN. The Raman spectra of the as-prepared materials is characterised by two main bands; the graphitic (G) band, which occurs at $\sim$1600 cm^{-1}; and the disordered (D) band, which occurs $\sim$1350 cm^{-1}. As shown in Fig. S9, the PAN powder does not show D and G bands while the electrospun PAN fibers show intense D and G bands characteristic of highly ordered material. When the electrospun fibers are doped with $Fe(acac)_3$, $Co(acac)_2$, and $Ni(acac)_2$, the resulting nanofibers shift the D and G bands to higher wavenumbers. The shift of the D and G bands can be attributed to the formation of metal oxides on fibers after pre-carbonisation treatment (Fe/Co/Ni_after PT). During the carbonisation of the PAN, H_2 is released which can reduce the metal oxides present to form metal nanoparticles. Meanwhile, CH_4 and CO are released during decomposition of PAN above 400 °C and these gases are dissociated at the surface of the metal catalytic domains, followed by carbon precipitation (via surface or volumetric diffusion) to initiate the CNT growth [33]. As seen from the SEM images (Figs. S1e, S1f, S2e S2f, S3e and S3f), the size of the Ni nanoparticles are larger than their Fe and Co based counterparts, resulting in the larger diameter of the grown CNT "bristle". This can be shown by the SEM images of the as-prepared carbon nanofibers (Figs. S1g, S1h, S2g, S2h, S3g and S3h), where the Ni based CMF have largest diameter "bristles".

Apart from the typical base- and tip-growth mode of CNTs, these structures also exhibit mixed-growth mechanisms that lead to peapod like carbon nanotubes with multiple metal domains. We therefore calculated the binding energies between different metal clusters and the CNT to further understand the CNT growth on the electrospun fibers. Here, the binding energies of Ni, Co and Fe clusters on CNTs were found to be −3.84 eV, −2.75 eV and −2.84 eV, respectively (Fig. S10). CNT growth may shift from base-growth to tip-growth with decreasing binding energy, indicating that Ni should show the strongest base growth mechanism while Co will experience more tip growth. This is experimentally confirmed from SEM images of their structures (Figs. S4 and S5). Interestingly, the peapod like carbon nanotubes as shown in Figs. S4b and S5b deviate from the above growth types. The mixed growth routes observed here can be attributed to use of carbon based substrates, which is conducive to metal diffusion (and floating catalyst). Compared to modelling results based on a Si substrate (Fig. S11), the binding energies of Ni, Co and Fe clusters on carbon based substrate are much smaller than those for the Si (111) surface [34] (−21.88 eV for Ni, −16.16 eV for Co, −13.24 eV for Fe). This weaker binding energy for Ni, Co and Fe on carbon indicates and the possibility of mixed growth mechanisms for all three carbon based materials, thus allowing the formation of the peapod structures. As can be seen in Fig. S5b, the CNT "bristles" formed via each different growth mechanism can be found in the same backbone fiber, where the tip- and base-growth can be seen together with peapod structures. More base-grown CNTs are found on Ni based fibers, as illustrated in Fig. S3h and as a result more peapod structures can also be found in Ni based fibers (Fig. S4).

Furthermore, density functional theory (DFT) calculations shows that the binding energies between the (111) surfaces of the Fe, Ni and Co with C6 were found to be −9.46 eV, −7.59 eV and −7.32 eV respectively (Table S3). This trend in binding energies between the metal domain and the carbon matches with observations in the thicknesses of carbon coatings on the nanoparticles. In the case of the Fe which has the strongest binding energy with the carbon, the thinnest carbon coating is observed. This suggests that once the first few layers of carbon are formed on the Fe it becomes difficult for additional carbon layers to be grown under this due to strong stabilisation (high binding energy) leading to difficulty in lifting the previous carbon layer up resulting in a relatively thin coating. In the case of the Ni and Co, which have similar binding energies, the thickness of the carbon coating is similar. Since the binding energy is lower than that of Fe, the growth of the carbon layers thus becomes easier as the initially formed carbon layer is more weakly bound. In addition, Jingde et al. [35] demonstrated that the energy barrier for carbon surface diffusion and carbon nucleation on the metals follows the order: Ni $\approx$ Co $<$ Fe, suggesting that carbon can diffuse and nucleate easily on surface of Ni and Co, which further indicates formation of a thicker carbon coating on their surface. In the TEM results, this thicker carbon layer thus results in a more graphitic domain close to the metal domain but a more amorphous region further from the metal domain which is likely due to stretching of the outer carbon layers during the coating growth leading to distortion of the graphitic domains.

Flexible Zn-air batteries via carbon metal fabrics. To demonstrate the potential of CMFs in electrochemical energy storage devices, we have designed and fabricated flexible rechargeable zinc-air batteries. All of the batteries are composed of a zinc metal foil anode, a PAN:poly(ethylene oxide) (PAN:PEO, 4:6) hydrogel electrolyte (Fig. S12), a pressed nickel foam current collector, and the free-standing CMF as the air cathodes. Fig. 5b shows the polarization and power density curves of the Fe 40% CMFs with "bristles" (mass loading of effective catalysis is about 10 wt% from Fig. S13) and metal CMFs (without "bristles") having the same mass loading of Fe, and CNF without any Fe.

The CMFs with CNT bristles offer a 113% increase in power density when compared to the non-hairy Fe-added CNF, and a 297% increase when compared to the CNF with no Fe. This observation, together with morphology and structural characterisation is attributed to the CMF with bristles enhancing the nanoporous 3D carbon network by increasing the specific surface area, number of electron pathways and also providing a catalytic domain for oxygen evolution/reduction. Additionally, the metal CNF electrodes maintain a high open circuit voltage (OCV) of 1.25 V but can reach up to 1.45 V when CMFs are used (Fig. S14, picture of the OCV of 1.45 V for single cell and 2.99 V for two cells connected in series). Furthermore, these fabrics exhibit a lower charge-discharge voltage gap than that of the metal CNF, indicating the better rechargeability of the zinc-air batteries with CMFs as air cathode (Fig. 5a).

Furthermore, in assessing the electrochemical impedance spectra (EIS) for the different air cathodes, the Nyquist plots indicate a smaller charge transfer resistance for the CMFs in comparison to the other materials (Fig. 5c). Galvanostatic discharge-charge cycling curves for the flexible rechargeable zinc-air batteries at 0.5 mA cm^{-2} are then demonstrated with twisted electrodes and different curvatures of 0°, 90°, and 180° (Fig. 5f). Along with its high flexibility and better electrochemical performance compared to the metal CNFs, our CMF fabrics also offer a significant improvement in cycle life due to their favourable bifunctional catalytic properties and increased specific surface area. As shown in Fig. S15, the calculated BET surface area of the Fe 40 CMFs with "bristles" (118.6 m^2/g) is higher than Fe 40 CMFs without "bristles" (35.5 m^2/g). Similarly, the calculated BET surface area of Fe 50 CMFs with "bristles" (282.8 m^2/g) is higher than Fe 50 CMFs without "bristles" (181.1 m^2/g). Fig. 5d demonstrates the stable galvanostatic cycling performance of the Fe based fabrics (10 min charge and 10 min discharge for each cycle), which outperform the metal CNF electrodes at the current density of 0.5 mA cm^{-2}. SEM analysis of the CMF electrodes after one cycle and 135 h charge/discharge cycles are

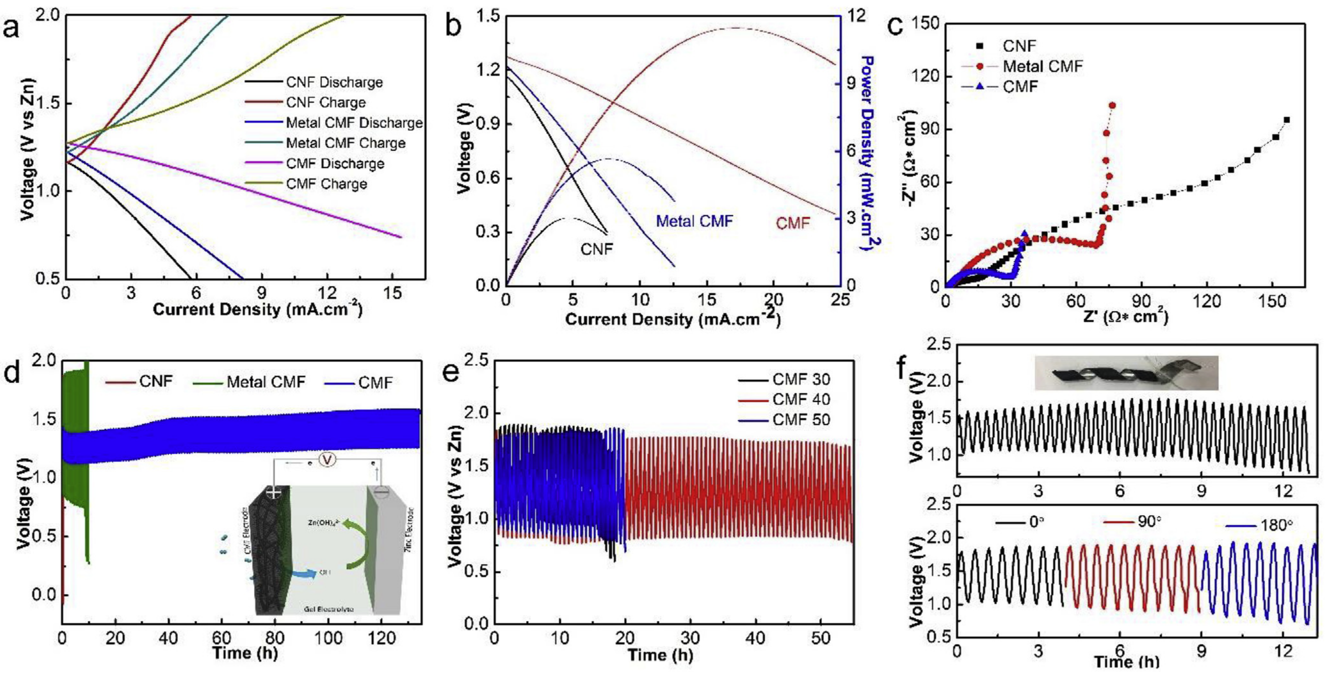

Fig. 5. Fe based CMF applied for Zn-air battery. a, Charge and discharge polarization curves of flexible rechargeable zinc-air batteries with different air cathodes. b, Polarization and power density curves of flexible rechargeable zinc-air batteries with different air cathodes. c, Nyquist plots of the impedance of the flexible rechargeable zinc-air batteries in the frequency range of 500 kHz to 0.05 Hz d, Galvanostatic discharge-charge cycling curves at 0.5 mA cm^{-2} for the flexible rechargeable zinc-air batteries for different air cathodes (insert schematic of Zn-Air battery with CMFs). e, Galvanostatic discharge-charge cycling curves at 0.5 mA cm^{-2} for the flexible rechargeable zinc-air batteries for different air cathodes with different Fe concentration. f, flexible and twistable flexible rechargeable zinc-air battery.

shown in Fig. S16, where the deposition of discharge products are found to be well confined within these fabrics and the battery failure is mainly attributable to the electrolyte evaporation. In this regard, Fig. S17 shows the atomic Hirshfeld charge distribution of a Fe atom inside the CNT, which highlights the possible ability of this material to help delocalize the charge distribution. The concentration of the Fe catalytic domains in the fabrics can also be directly controlled to 30%, 40% and 50% as shown in Fig. 5e where the Fe40 CMFs achieve the best cycling stability for nearly 60 h of cycling a current density of 0.5 mA cm^{-2} (15 min charge and 15 min discharge for each cycle). The assembled Zn-air batteries also show good performance even when the battery is twisted into a spiral shape (Fig. 5f) and can be operated under different bending conditions without compromising on their electrochemical performance (Fig. S18). Compared to the recently reported flexible Zn-air batteries (Table S3), CMFs based Zn-air battery can achieve comparable electrochemical performance, while being fully mechanically flexible.

The flexible battery application can be extended to Ni CMFs and Co CMFs. As shown in Fig. 5e and Fig. S19, Fe 50 CMFs, Ni 50 CMFs and Co 50 CMFs all show good cycling performances in Zn-air batteries. These electrochemical enhancements demonstrate the advantage of CMFs with fine CNT "bristles", which can increase the surface area, facilitate electrochemical reactions and promote uninterrupted pathways for oxygen diffusion across electrodes. The various metal additives are partly oxidized before cycling and can be further oxidized during the cycling process, and these catalytic metal oxide particles can contribute to battery performance. Both Raman spectra and XRD patterns prove the presence of partly oxidized metal catalysts before cycling and enhanced oxidation after cycling as shown in Fig. S20 and Fig. S21.

In conclusion, we present a tractable route to manufacture non-woven carbon fabrics made up of electrospun carbon fibers bearing carbon nanotube bristles that contain catalytically active metal nanoparticles without activating catalyst and introducing extra carbon source. Our microscopic, spectroscopic and modelling has shown that these self-assembling hierarchical structures come about through the decomposition and exsolution of low-cost acetylacetonate salts of Ni, Co and Fe which form surface nanoparticles on electrospun and heat treated PAN fibers in air. Further, carbonisation results in CNT "bristle" growth in N_2 where the carbon source is provided by the decomposition products of the PAN resulting in CMFs which have a combination of base-growth, tip-growth and peapod like structures due to the low binding energy of the metal to the CNF. The metallic domains are all coated in a carbon layer which is found to have a graphitic core region and disordered shell region. The partly oxidized metallic domains appear to have a beneficial effect on catalytic performances of CMFs. Therefore these free standing, mechanically flexible and twistable fabrics can be used as electrodes for next generation energy storage devices. As a proof of concept, these CMFs were utilized as air cathodes in a flexible Zn-air battery, resulting in double the power density when benchmarked against pure carbon fibers.

1. Experimental section

CMFs production: The precursor solution was first prepared by mixing 0.8 g Iron (III) acetylacetonate $Fe(acac)_3$ and 12 ml DMF (Fig. 1a upper photo), followed by adding 1.2 g of PAN, whereby a dark orange solution was obtained after magnetic stirring the mixture at 55 °C for 24 h (Fig. 1a lower photo). For the electrospinning process, the as-prepared precursor solution was transferred to a syringe and driven into the electrospinning needle at 1.5 ml/h by a syringe pump. The needle (19 G, double) was held at 13 kV provided by a high voltage power supply (GenVolt 73030), with a working distance of 20 cm from the grounded rotating collector (rotating speed 2000 RPM, 25 °C, 50% humidity). An orange coloured electrospun nanofiber film is produced via this process, as shown in Fig. 1a. Following the same preparation process, Cobalt (II) acetylacetonate (Co(acac)2) and Nickel (II) acetylacetonate $Ni(acac)_2$ were also used to create nanofiber films. Their mixtures with DMF (Fig. 1b and c, upper) and DMF + PAN (Fig. 1b and c, lower) were electrospun resulting in pink coloured $Co(acac)^2$ doped PAN nanofibers and green colour $Ni(acac)_2$ doped PAN nanofiber films.

The as-prepared nanofibers were peeled off the aluminium foil attached to the rotating collector and the Fe/Co/Ni based nanofiber films were stabilised at 290 °C in air for 2 h with a ramp rate of 2 °C min^{-1}. Then the films were fully carbonised at 850 °C in N_2 (initial ramp rate of 2 °C min^{-1}, dwell time of 2 h at 300 °C, ramp rate of 5 °C min^{-1} to 850 °C, dwell time 2 h). On completion of the heat treatment, growth of carbon nano-hairs with metallic catalytic domains on the electrospun fabrics were achieved. SEM images are shown in Fig. 1d and g for Fe based fabric, Fig. 1e and h for Co based fabrics, and Fig. 1f and i for Ni based HCNF show the hierarchical micro/nanostructure which resembling fine bristles found in certain plants and insects. These Fe, Co and Ni based nanotubes have diameters approximately of 10–50 nm and up to several hundred nanometers (approximately 600 nm) in length. Compared to other preparation methods (Table S1), our CMF can be obtained, via a facile preparation method without catalyst deposition, catalyst activation and without an additional carbon source being introduced.

Declaration of competing interest

The authors declare that they have no known competing financial interests or personal relationships that could have appeared to influence the work reported in this paper.

CRediT authorship contribution statement

Xinhua Liu: Conceptualization, Writing - original draft. **Mengzheng Ouyang:** Methodology. **Marcin W. Orzech:** Data curation. **Yubiao Niu:** Data curation. **Weiqiang Tang:** Data curation. **Jingyi Chen:** Data curation. **Max Naylor Marlow:** Data curation. **Debashis Puhan:** Data curation. **Yan Zhao:** Data curation. **Rui Tan:** Data curation. **Brankin Colin:** Data curation. **Nicholas Haworth:** Data curation. **Shuangliang Zhao:** Methodology. **Huizhi Wang:** Methodology, Funding acquisition. **Peter Childs:** Supervision. **Serena Margadonna:** Supervision, Funding acquisition. **Marnix Wagemaker:** Supervision. **Feng Pan:** Supervision, Funding acquisition. **Nigel Brandon:** Supervision. **Chandramohan George:** Writing - review & editing, Funding acquisition. **Billy Wu:** Writing - review & editing, Supervision, Project administration, Funding acquisition.

Acknowledgements

This work was kindly supported by the EPSRC energy storage for low carbon grids project (EP/K002252/1), the EPSRC Joint UK-India Clean Energy Centre (JUICE) (EP/P003605/1), the EPSRC Multi-Scale Modelling project (EP/S003053/1), and the Innovate UK for Advanced Battery Lifetime Extension (ABLE) project, Soft Science Research Project of Guangdong Province (No. 2017B030301013), Shenzhen Science and Technology Research Grant (ZDSYS201707281026184). Swansea University College of Engineering Advanced Imaging of Materials (AIM) Facility, which was funded by the EPSRC (EP/M028267/1), the European Regional Development Fund through the Welsh Government (80708), and the Ser Solar project via Welsh Government. CG acknowledges The Royal Society of London for an URF. X. Liu and M. Ouyang contribute equally to this work.

Appendix A. Supplementary data

Supplementary data to this article can be found online at https://doi.org/10.1016/j.ensm.2020.04.001.

References

[1] L. Dai, D.W. Chang, J.B. Baek, W. Lu, Carbon nanomaterials for advanced energy conversion and storage, Small (2012), https://doi.org/10.1002/smll.201101594.

[2] S.L. Candelaria, Y. Shao, W. Zhou, X. Li, J. Xiao, J.G. Zhang, Y. Wang, J. Liu, J. Li, G. Cao, Nanostructured carbon for energy storage and conversion, Nanomater. Energy (2012), https://doi.org/10.1016/j.nanoen.2011.11.006.

[3] S. Iijima, Nature 354 (1991) 56, https://doi.org/10.1038/354056a0, pdf, (n.d.).

[4] B.J. Landi, M.J. Ganter, C.D. Cress, R.A. DiLeo, R.P. Raffaelle, Carbon nanotubes for lithium ion batteries, Energy Environ. Sci. (2009), https://doi.org/10.1039/b904116h.

[5] S. Wu, R. Xu, M. Lu, R. Ge, J. Iocozzia, C. Han, B. Jiang, Z. Lin, Graphene-containing nanomaterials for lithium-ion batteries, Adv. Energy Mater. (2015), https://doi.org/10.1002/aenm.201500400.

[6] J. Zhang, Z. Xia, L. Dai, Carbon-based electrocatalysts for advanced energy conversion and storage, Sci. Adv. (2015), https://doi.org/10.1126/sciadv.1500564.

[7] I.V. Lightcap, P.V. Kamat, Graphitic design: prospects of graphene-based nanocomposites for solar energy conversion, storage, and sensing, Acc. Chem. Res. (2013), https://doi.org/10.1021/ar300248f.

[8] X. Li, Y. Chen, H. Huang, Y.W. Mai, L. Zhou, Electrospun carbon-based nanostructured electrodes for advanced energy storage - a review, Energy Storage Mater (2016), https://doi.org/10.1016/j.ensm.2016.06.002.

[9] C. Wang, M. Waje, X. Wang, J.M. Tang, R.C. Haddon, Y. Yan, Proton exchange membrane fuel cells with carbon nanotube based electrodes, Nano Lett. (2004), https://doi.org/10.1021/nl034952p.

[10] W. Li, F. Zhang, Y. Dou, Z. Wu, H. Liu, X. Qian, D. Gu, Y. Xia, B. Tu, D. Zhao, A self-template strategy for the synthesis of mesoporous carbon nanofibers as advanced supercapacitor electrodes, Adv. Energy Mater. (2011), https://doi.org/10.1002/aenm.201000096.

[11] Z. Li, J.T. Zhang, Y.M. Chen, J. Li, X.W. Lou, Pie-like electrode design for high-energy density lithium-sulfur batteries, Nat. Commun. (2015), https://doi.org/10.1038/ncomms9850.

[12] B. Zhang, F. Kang, J.M. Tarascon, J.K. Kim, Recent advances in electrospun carbon nanofibers and their application in electrochemical energy storage, Prog. Mater. Sci. (2016), https://doi.org/10.1016/j.pmatsci.2015.08.002.

[13] S. Cavaliere, S. Subianto, I. Savych, D.J. Jones, J. Rozière, Electrospinning: designed architectures for energy conversion and storage devices, Energy Environ. Sci. (2011), https://doi.org/10.1039/c1ee02201f.

[14] H.G. Wang, S. Yuan, D.L. Ma, X.B. Zhang, J.M. Yan, Electrospun materials for lithium and sodium rechargeable batteries: from structure evolution to electrochemical performance, Energy Environ. Sci. (2015), https://doi.org/10.1039/c4ee03912b.

[15] X. Liu, M. Naylor Marlow, S.J. Cooper, B. Song, X. Chen, N.P. Brandon, B. Wu, Flexible all-fiber electrospun supercapacitor, J. Power Sources 384 (2018), https://doi.org/10.1016/j.jpowsour.2018.02.081.

[16] K. Liu, W. Liu, Y. Qiu, B. Kong, Y. Sun, Z. Chen, D. Zhuo, D. Lin, Y. Cui, Electrospun core-shell microfiber separator with thermal-triggered flame-retardant properties for lithium-ion batteries, Sci. Adv. (2017), https://doi.org/10.1126/sciadv.1601978.

[17] C. Zhu, Y. Yu, L. Gu, K. Weichert, J. Maier, Electrospinning of highly electroactive carbon-coated single-crystalline LiFePO4 nanowires, Angew. Chem. Int. Ed. (2011), https://doi.org/10.1002/anie.201005428.

[18] X. Xiong, W. Luo, X. Hu, C. Chen, L. Qie, D. Hou, Y. Huang, Flexible membranes of MoS2/C nanofibers by electrospinning as binder-free anodes for high-performance sodium-ion batteries, Sci. Rep. (2015), https://doi.org/10.1038/srep09254.

[19] Q. Liu, Y. Wang, L. Dai, J. Yao, Scalable fabrication of nanoporous carbon fiber films as bifunctional catalytic electrodes for flexible Zn-air batteries, Adv. Mater. 28 (2016) 3000–3006, https://doi.org/10.1002/adma.201506112.

[20] K.N. Jung, S.M. Hwang, M.S. Park, K.J. Kim, J.G. Kim, S.X. Dou, J.H. Kim, J.W. Lee, One-dimensional manganese-cobalt oxide nanofibres as bi-functional cathode catalysts for rechargeable metal-air batteries, Sci. Rep. (2015), https://doi.org/10.1038/srep07665.

[21] N. Iqbal, X. Wang, A.A. Babar, G. Zainab, J. Yu, B. Ding, Flexible Fe3O4@carbon nanofibers hierarchically assembled with MnO2 particles for high-performance supercapacitor electrodes, Sci. Rep. (2017), https://doi.org/10.1038/s41598-017-15535-x.

[22] N. Radacsi, F.D. Campos, C.R.I. Chisholm, K.P. Giapis, Spontaneous formation of nanoparticles on electrospun nanofibres, Nat. Commun. (2018), https://doi.org/10.1038/s41467-018-07243-5.

[23] Y. Liu, J. Luo, C. Helleu, M. Behr, H. Ba, T. Romero, A. Hébraud, G. Schlatter, O. Ersen, D.S. Su, C. Pham-Huu, Hierarchical porous carbon fibers/carbon nanofibers monolith from electrospinning/CVD processes as a high effective surface area support platform, J. Mater. Chem. A. 5 (2017) 2151–2162, https://doi.org/10.1039/c6ta09414g.

[24] S. Zhang, H. Liu, N. Tang, J. Ge, J. Yu, B. Ding, Direct electronetting of high-performance membranes based on self-assembled 2D nanoarchitectured networks, Nat. Commun. (2019), https://doi.org/10.1038/s41467-019-09444-y.

[25] C. Lai, Q. Guo, X.F. Wu, D.H. Reneker, H. Hou, Growth of carbon nanostructures on carbonized electrospun nanofibers with palladium nanoparticles, Nanotechnology 19 (2008), https://doi.org/10.1088/0957-4484/19/19/195303.

[26] Y. Yao, Z. Huang, P. Xie, S.D. Lacey, R.J. Jacob, H. Xie, F. Chen, A. Nie, T. Pu, M. Rehwoldt, D. Yu, M.R. Zachariah, C. Wang, R. Shahbazian-Yassar, J. Li, L. Hu, Carbothermal shock synthesis of high-entropy-alloy nanoparticles, Science 359 (2018) 1489–1494, https://doi.org/10.1126/science.aan5412 (80-.).

[27] Y. Zhao, J. Zhang, X. Guo, H. Fan, W. Wu, H. Liu, G. Wang, Fe3C@nitrogen doped CNT arrays aligned on nitrogen functionalized carbon nanofibers as highly efficient catalysts for the oxygen evolution reaction, J. Mater. Chem. A. 5 (2017) 19672–19679, https://doi.org/10.1039/c7ta05936a.

[28] Y. Chen, X. Li, K.S. Park, J. Hong, J. Song, L. Zhou, Y.W. Mai, H. Huang, J.B. Goodenough, Sulfur encapsulated in porous hollow CNTs@CNFs for high-

performance lithium-sulfur batteries, J. Mater. Chem. A. 2 (2014) 10126–10130, https://doi.org/10.1039/c4ta01823k.
[29] Y. Chen, X. Li, K. Park, J. Song, J. Hong, L. Zhou, Y.W. Mai, H. Huang, J.B. Goodenough, Hollow carbon-nanotube/carbon-nanofiber hybrid anodes for Li-ion batteries, J. Am. Chem. Soc. 135 (2013) 16280–16283, https://doi.org/10.1021/ja408421n.
[30] J. Maire, J. Mering, Graphitization of Soft carbons, Chem. Phys. Soft Carbons. 6 (1970) 125–190.
[31] J. Donnet, O. Bahl, Encyclopedia of Physical Science and Technology, vol. 2, Acedamic Press Inc., New York, 1987.
[32] Y. Li, M. Afzaal, P. O'Brien, The synthesis of amine-capped magnetic (Fe, Mn, Co, Ni) oxide nanocrystals and their surface modification for aqueous dispersibility, J. Mater. Chem. 16 (2006) 2175–2180, https://doi.org/10.1039/b517351e.
[33] M.S.A. Rahaman, A.F. Ismail, A. Mustafa, A review of heat treatment on polyacrylonitrile fiber, Polym. Degrad. Stabil. 92 (2007) 1421–1432, https://doi.org/10.1016/j.polymdegradstab.2007.03.023.
[34] K. Kordás, A.E. Pap, J. Vähäkangas, A. Uusimäki, S. Leppävuori, Carbon nanotube synthesis on oxidized porous silicon, Appl. Surf. Sci. 252 (2005) 1471–1475, https://doi.org/10.1016/j.apsusc.2005.02.120.
[35] J. Li, E. Croiset, L. Ricardez-Sandoval, Carbon nanotube growth: first-principles-based kinetic Monte Carlo model, J. Catal. 326 (2015) 15–25, https://doi.org/10.1016/j.jcat.2015.03.010.